Three-Dimensional Imaging of Colloidal Glasses under Steady Shear

R. Besseling,[1] Eric R. Weeks,[2] A. B. Schofield,[1] and W. C. K. Poon[1]

[1]*Scottish Universities Physics Alliance (SUPA) and School of Physics, The University of Edinburgh, Kings Buildings, Mayfield Road, Edinburgh EH9 3JZ, United Kingdom*

[2]*Physics Department, Emory University, Atlanta, Georgia 30322, USA*

(Received 9 May 2006; revised manuscript received 27 February 2007; published 9 July 2007)

Using fast confocal microscopy we image the three-dimensional dynamics of particles in a yielded hard-sphere colloidal glass under steady shear. The structural relaxation, observed in regions with uniform shear, is nearly isotropic but is distinctly different from that of quiescent metastable colloidal fluids. The inverse relaxation time τ_α^{-1} and diffusion constant D, as functions of the *local* shear rate $\dot{\gamma}$, show marked shear thinning with $\tau_\alpha^{-1} \propto D \propto \dot{\gamma}^{0.8}$ over more than two decades in $\dot{\gamma}$. In contrast, the *global* rheology of the system displays Herschel-Bulkley behavior. We discuss the possible role of large scale shear localization and other mechanisms in generating this difference.

DOI: 10.1103/PhysRevLett.99.028301 PACS numbers: 82.70.−y, 83.50.−v, 83.60.−a, 83.80.Hj

Glassy materials are ubiquitous in nature and in industry, e.g., molecular and metallic glasses [1,2] and soft glasses [3,4] like colloidal suspensions. Of special interest is their rheology. Glasses have liquidlike microstructure, but solidlike mechanical behavior. At low applied stress, they have finite shear moduli, but at larger stress they yield and display highly nonlinear flow behavior.

Even the simplest form of *nonlinear* glassy rheology, steady shear, is far from fully understood. Various theoretical mechanisms are proposed [4–7] for shear-induced relaxation of arrested matter, predicting a variety of constitutive relations. Significantly, all these theories assume globally uniform shear. Simulations, so far the main tool to check directly the relation between microscopic behavior and macroscopic flow, reveal spatially heterogeneous relaxation [7,8] and strong shear thinning [9,10]. Experiments are just starting to address microscopic dynamics under shear, but have been limited to coarse-grained data, two dimensional (2D) or interrupted flows, or ordering phenomena [11–14]. Moreover, experiments imaging *global* flow [15] as well as boundary driven simulations of Lennard-Jones (LJ) glasses [16] show that (soft) glasses often exhibit shear localization, which cannot be described by simple constitutive laws.

Here we report a three-dimensional (3D) imaging study of microscopic relaxation in a colloidal glass under steady shear. The relaxation rate τ_α^{-1} and the diffusion constant D are nearly isotropic and show marked shear thinning as a function of the *local* shear rate $\dot{\gamma}$: $\tau_\alpha^{-1} \propto D \propto \dot{\gamma}^{0.8}$. The latter contrasts significantly with the *global* rheology, which shows Herschel-Bulkley behavior.

We used sterically stabilized polymethylmethacrylate colloids (radius $a = 850$ nm, measured by light scattering, polydispersity $\lesssim 10\%$ [17]) dyed with nitrobenzoxadiazole and suspended in cycloheptyl bromide mixed with decalin for density and refractive index matching. In this medium colloids have a small charge [18] which we screen by adding 4 mM tetrabutylammoniumchloride, giving nearly hard-sphere (HS) behavior and a glass transition at volume fraction $\phi_g \simeq 0.58$ (determined from mean-squared displacements) [19]; we work at $\phi \simeq 0.62$ (measured by imaging). The reduced shear rate, or Péclet number, is $\mathrm{Pe} = 4a^2\dot{\gamma}/D_0 = 24\dot{\gamma}\tau_B$, with D_0 the bare diffusion coefficient and $\tau_B = 1.24$ s the Brownian time in our system.

We used a linear parallel-plate shear cell with a plate separation ~400–800 μm, parallel to ± 5 μm over a ~200 mm^2 drop of colloid confined between the plates by surface tension. We define x, y, and z as the velocity, vorticity (or neutral), and gradient directions, respectively. The top plate is driven at 0.05–10 μm/s by a mechanical actuator with magnetic encoder and steady shear is applied up to a total accumulated strain $\Delta\gamma \simeq 1000\%$. Wall slip and wall-induced ordering were prevented by coating the slides with 1–3 disordered layers of colloid. A solvent bath minimized evaporation.

A $30 \times 30 \times 15$ μm^3 volume in the drop, with $N \sim 3000$ colloids, was imaged from below as a stack of 75 slices using a fast confocal scanner (VT-Eye, Visitech Int.). Each stack acquisition took 1.7 s. Colloids were located to ± 30 nm in x, y, and ± 90 nm in z [21]. Tracking from frame to frame was achieved by first subtracting from the raw coordinates a time dependent x-displacement profile $\Delta x(z, t)$, measured via correlation analysis of raw images, and adding this back after particle tracking [22]. The resulting x displacements over a given time dt, $\{\Delta x_i(z_i, dt)\}$ ($i = 1$ to N), always have an average linear dependence on z, demonstrating uniform shear in our imaged volume. We measured the actual (local) shear rate $\dot{\gamma}$, which may differ from the applied (global) rate $\dot{\gamma}_a$ due to shear localization and the presence of jammed regions. We will return to this point; for now we focus on steady states with uniform shear in a region from 15–30 μm above the cover slide. When present, strong decay in $\dot{\gamma}$ occurs at least $\Delta z \sim 20a$ away from imaged regions. We also checked, via bond-order analysis [23], that shear crystallization [24] was absent for $\dot{\gamma} \lesssim 0.1$ s^{-1}.

Figure 1(a) displays the trajectories in an x, z slice at $\dot{\gamma} = 0.93 \times 10^{-3}$ s^{-1}, showing the displacement gradi-

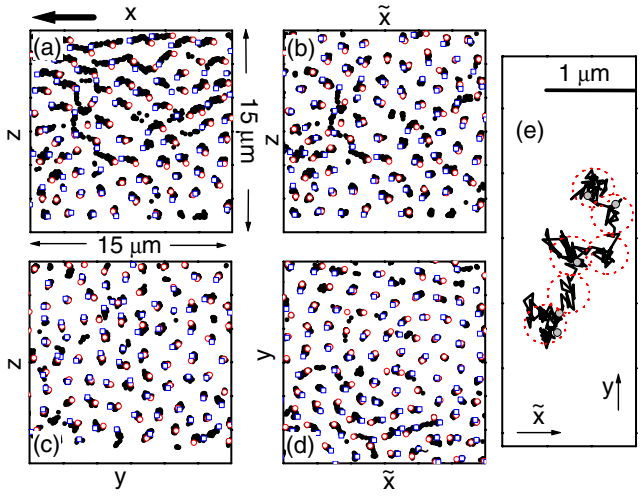

FIG. 1 (color online). Colloid trajectories for $\dot{\gamma} = 9.3 \times 10^{-4}\ \mathrm{s}^{-1}$. (a) 1.5 μm thick slice in the x, z plane for 160 s. The start of each trajectory is shown by ○, the end by □. The big arrow marks the shear direction. (b) As in (a) but in the desheared, $\tilde{x}$, z, reference frame, with $\tilde{x}_i = x_i - \dot{\gamma} \int_0^t z_i(t')\, dt'$. (c) y, z plane over 160 s. (d) $\tilde{x}$, y plane over 160 s. (e) Single trajectory in the $\tilde{x}$, y plane over 800 s. Dotted circles mark rattling in several cages (*not* the particle size), gray dots show the locations at $t = 0$, 200, 400, 600, 800 s.

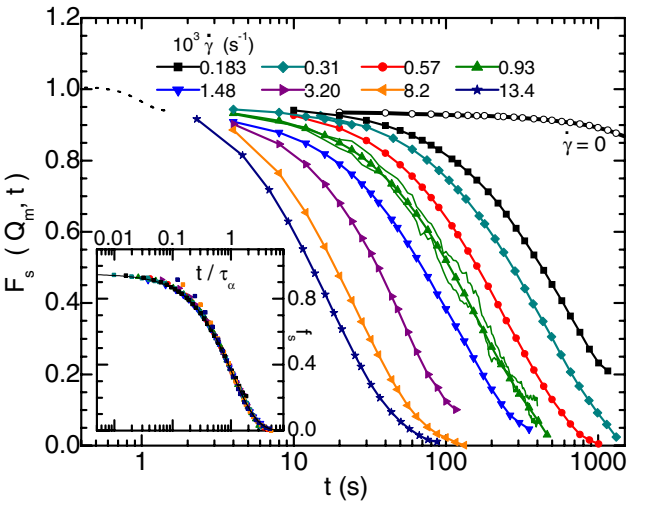

FIG. 2 (color online). Selected incoherent scattering functions $F_s(Q_m, t)$, with $\dot{\gamma}$ increasing from right to left. Lines for $\dot{\gamma} = 0.93 \times 10^{-3}\ \mathrm{s}^{-1}$ show two curves used in the average with start times t_0 spaced by 180 s. The dashed line schematizes initial relaxation. Inset: data collapse using $f_s(Q_m, t/\tau_\alpha)$. Line: $f_s \propto \exp(-t/\tau_\alpha)$.

ent due to shear. To highlight the shear-induced dynamics, we show in Fig. 1(b) the *nonaffine* displacements obtained by subtracting the uniform shear via $\tilde{x}_i = x_i - \dot{\gamma} \int_0^t z_i(t')\, dt'$. Considerable nonaffine displacements are seen in this and other planes, Figs. 1(c) and 1(d). On the time scale considered here, these rearrangements are heterogeneous, somewhat similar to the *quiescent* dynamics in dense colloidal fluids with $\phi < \phi_g$ [25]. Focusing on a single particle, Fig. 1(e), we see that its dynamics under shear consists of intervals of cage "rattling," interrupted by shear-induced cage-breaking events.

Next, we study the relaxation via the incoherent scattering function, $F_s(Q, t) = \langle \cos(Q[y_i(t_0 + t) - y_i(t_0)]) \rangle_{i,t_0}$, at a scattering vector $Q = Q_m \simeq 3.8a^{-1}$ where the data's structure factor $S(Q)$ shows a peak. In Fig. 2 we show selected results for $\vec{Q} \parallel y$, but the results (not shown) for $\vec{Q} \parallel z$ and x, using the nonaffine displacements $\tilde{x}_i$ for the latter, are similar. F_s for the quiescent glass ($\dot{\gamma} = 0$) hardly decays over our observation window, reflecting the caging of particles by their neighbors; at longer times we observed aging (data not shown) [14,26]. The short time decay due to initial cage exploration ($t \lesssim \tau_B$ [20], dashed line in Fig. 2) is inaccessible to us. At small $\dot{\gamma}$, F_s at short times still exhibits a plateau, in agreement with the caging in Fig. 1(e). As $\dot{\gamma}$ increases, this plateau shrinks and for the highest $\dot{\gamma}$ it vanishes and likely merges with the short time decay. At longer times, F_s decays strongly for all $\dot{\gamma} \neq 0$, marking shear-induced structural relaxation and cage rearrangements. The structural relaxation time τ_α, defined by $F_s(Q_m, t = \tau_\alpha) = e^{-1}$, decreases on increasing $\dot{\gamma}$. Importantly, F_s is independent of the starting time t_0 (see data for $\dot{\gamma} = 0.93 \times 10^{-3}\ \mathrm{s}^{-1}$); i.e., a stationary state is achieved.

Our data confirm the theoretically predicted "time-shear superposition principle" [5,6]: when time is scaled by τ_α, the α relaxation follows a master curve $f_s(Q_m, t/\tau_\alpha)$, Fig. 2 inset. As in LJ simulations [9], our f_s is a pure exponential. This differentiates a shear-melted glass from a concentrated HS colloidal fluid at $\phi < \phi_g$ and $\dot{\gamma} = 0$, where we find a stretched exponential behavior for $F_s(Q \gtrsim Q_m/2)$, as can also be deduced from [20].

We find that $\tau_\alpha \propto \dot{\gamma}^{-\nu}$ with $\nu = 0.80 \pm 0.01$ [27], independent of the criterion or Q used to determine τ_a. This behavior means that the accumulated strain at τ_α is not constant, but varies as $\dot{\gamma}\tau_\alpha \propto \dot{\gamma}^{0.2}$. These data are consistent with a schematic model [5] for driven glasses and also match the "creep" of a driven particle in a correlated random potential [28]. An "entropic barrier hopping" model [29], without any "ideal" glass divergences, shows a similar dependence of the hopping time on $\dot{\gamma}$.

Turning to the mean-squared displacement (MSD) $\langle dy^2(t) \rangle$, Fig. 3(a) inset, we see that it exhibits a crossover from caged to diffusive motion for $\sqrt{\langle dy^2 \rangle}/a \simeq 0.15$ ($\langle dy^2 \rangle \simeq 0.017\ \mu\mathrm{m}^2$), consistent with the "Lindemann parameter" for cage rattling at the quiescent glass transition [19]. The long time self-diffusion constant D_y, Fig. 3(b), follows the relaxation rate $D_y \propto \tau_\alpha^{-1} \propto \dot{\gamma}^{0.8}$, and *not* the shear rate $\dot{\gamma}$. To emphasize this and to address anisotropy in the dynamics, we plot in Fig. 3(c) the product $2D_j\tau_\alpha$ for $j = x$, y, z along with the value $\langle dy^2(\tau_\alpha) \rangle = 2/Q_m^2$ expected from a Gaussian approximation $F_s(Q_m, t) \simeq e^{-Q_m^2 \langle dy^2(t) \rangle/2}$ [20]. We find that $Q_m^2 D_y \tau_\alpha \approx 1.1$ and this also holds for $j = x$, z [30]. We again stress the difference

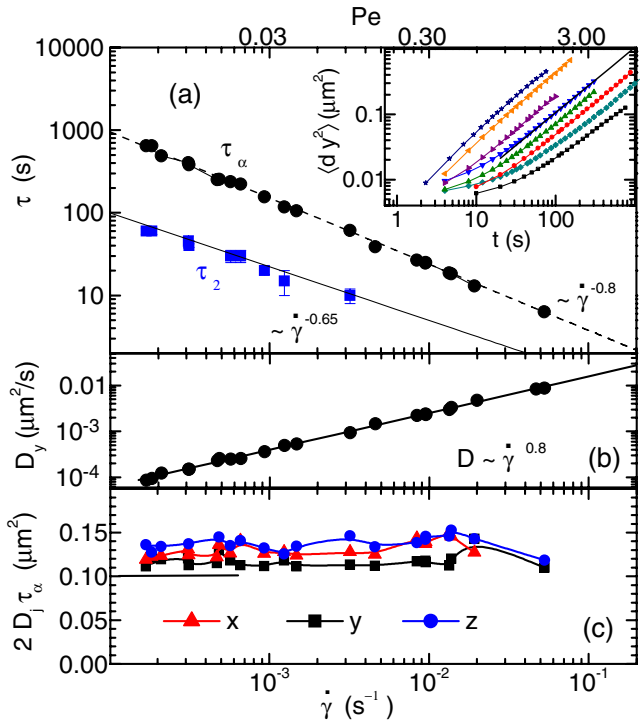

FIG. 3 (color online). (a) Relaxation time (●) and the time τ_2 characterizing the crossover from caged to diffusive behavior (■) vs $\dot{\gamma}$; dashed line: $\tau_\alpha \propto \dot{\gamma}^{-0.8}$; full line: $\tau_2 \propto \dot{\gamma}^{-0.65}$. Inset: y-mean-squared displacement for shear rates as in Fig. 2. Line: $\langle dy^2(t)\rangle = 2D_y t$ for $\dot{\gamma} = 1.48 \times 10^{-3}$ s^{-1}. (b) (●) Diffusion constant D_y vs $\dot{\gamma}$. Line: $D_y \propto \dot{\gamma}^{0.8}$. (c) The scaled diffusion constant $2D_j\tau_\alpha \simeq \langle dr_j^2(\tau_\alpha)\rangle$ vs $\dot{\gamma}$ for $j = x, y, z$. Line: the value $\langle dy^2(\tau_\alpha)\rangle = 2/Q_m^2$ expected for Gaussian behavior.

with quiescent fluids at $\phi < \phi_g$, which always show $D\tau_\alpha < Q^{-2}$ for $Q \gtrsim Q_m$. Figure 3(c) also shows that the diffusion constants exhibit only a mild anisotropy: while $D_z > D_{x,y}$, the difference is $\lesssim 20\%$. Similar or even smaller anisotropy has been observed in simulations of sheared glasses [8,10] and colloidal fluids [31], and in experiments on *dilute* suspensions [32]. However, sheared *non-Brownian* suspensions (Pe $\to \infty$) show strong anisotropy ($D_x^\infty / D_{y,z}^\infty \sim 8$) [33], with $D^\infty \propto \dot{\gamma}$.

As a last microscopic characterization we study the probability distribution of displacements $P[dy(t)]$ and the non-Gaussian parameter $\alpha_{2,y} = \langle dy^4(t)\rangle / 3\langle dy^2(t)\rangle^2 - 1$. The latter measures broad tails in $P[dy(t)]$, reflecting cage rearrangements as in Fig. 1(e). Figure 4(a) shows $\alpha_{2,y}(t)$ for various $\dot{\gamma}$. It peaks at $t \equiv \tau_2$ corresponding to the crossover from caged to diffusive behavior in the MSD [inset, Fig. 3(a)], and vanishes for $t \gtrsim \tau_\alpha$. A nonzero α_2 also suggests cooperative motion, consistent with the heterogeneities for $t \lesssim \tau_\alpha$ in Figs. 1(b)–1(d). The peak time follows $\tau_2 \propto \dot{\gamma}^{0.65}$, Fig. 3(a), somewhat different from the τ_α scaling. Interestingly, the distributions $P\{dy[t = \tau_2(\dot{\gamma})]\}$ nearly collapse for different $\dot{\gamma}$ [Fig. 4(b)], despite a slight decrease of $\alpha_2(\tau_2)$ with $\dot{\gamma}$. In quiescent systems at $\phi < \phi_g$, such (near) collapse of $P\{dy[\tau_2(\phi)]\}$ at different ϕ is *not* expected since there $\alpha_2(\tau_2)$ grows strongly with ϕ while the MSD at τ_2 decreases rapidly [25].

We now return to the $\dot{\gamma}$ dependence of τ_α. There is currently no firm theoretical basis for relating τ_α to flow properties. Nevertheless, τ_α is often taken (with some simulational evidence [34]) as proportional to viscosity [6], giving an effective stress $\bar{\sigma} = G_0\tau_\alpha\dot{\gamma}$ with G_0 a modulus. The resulting "microscopic" flow curve shows $\bar{\sigma} \propto \dot{\gamma}^{0.2}$, Fig. 5. Recent theories [4,6] have argued for the existence of a dynamic yield stress at $\dot{\gamma} \to 0^+$ in uniform shear. However, our results show no sign of a plateau in $\bar{\sigma}$ for reduced rates down to Pe $\simeq 0.005$.

Figure 5 shows the experimental *global* flow curve measured with a stress controlled rheometer (AR2000, TA Instruments) in cone-plate geometry (diameter 40 mm, angle 1°, both surfaces coated with particles). The stress σ is related to the average shear rate $\dot{\gamma}_a$ by $\sigma(\dot{\gamma}_a) = \sigma_Y^{(D)} + A\dot{\gamma}_a^n$ with a dynamic yield stress $\sigma_Y^{(D)} = 1.36$ Pa and $n = 0.56$, similar to previous HS measurements [35].

To compare with the local behavior $\bar{\sigma} = G_0\tau_\alpha\dot{\gamma}$, in Fig. 5 we have chosen G_0 to match $\bar{\sigma}$ and $\sigma(\dot{\gamma}_a)$ at high $\dot{\gamma}$. Clearly, the local and global data disagree. Some discrepancy may be due to the fact that, for Pe $\gtrsim 1$, hydrodynamic effects render the relation $\bar{\sigma} \propto \tau_\alpha\dot{\gamma}$ less valid. More importantly, discrepancy could arise from the presence of shear localization, e.g., due to the existence of a static yield stress [5,16]. We have already mentioned that in our parallel-plate shear cell, a global shear rate $\dot{\gamma}_a$ typically corresponds to a jammed region ($\dot{\gamma} \simeq 0$) coexisting with a flowing region with $\dot{\gamma} > \dot{\gamma}_a$. Preliminary flow imaging *inside* our rheometer shows that shear localization also occurs in the cone-plate geometry, and sets in for $\dot{\gamma}_a \leq 10^{-2}$ s^{-1} [36]. In LJ simulations [16], differences between $\dot{\gamma}$ and $\dot{\gamma}_a$ could indeed explain small deviations between

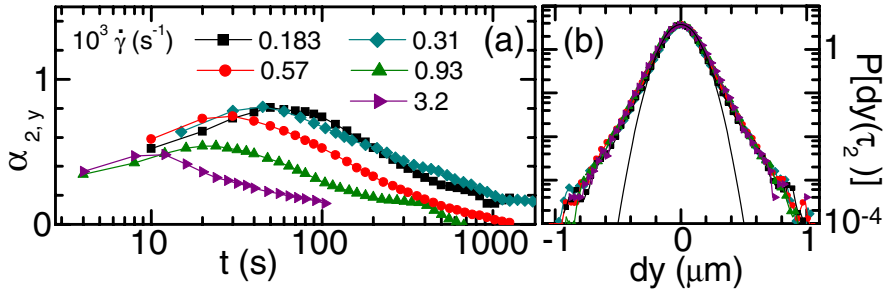

FIG. 4 (color online). (a) Non-Gaussian parameter $\alpha_2(t)$ of the probability distribution $P[dy(t)]$, for several shear rates. (b) $P[dy(t = \tau_2(\dot{\gamma}))]$ for the corresponding $\dot{\gamma}$, showing a near collapse of the data (each involving $>10^5$ displacements). Line: best Gaussian fit.

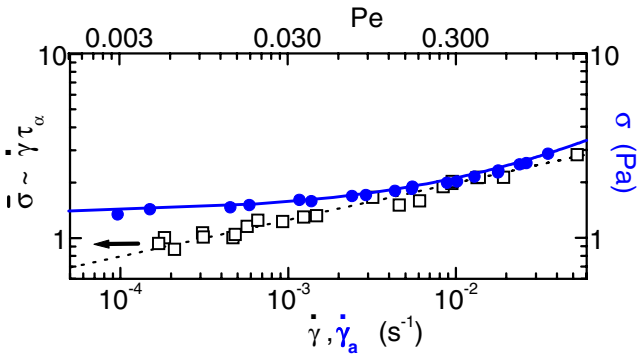

FIG. 5 (color online). (□) Local "flow curve" $\bar{\sigma} = G_0\dot{\gamma}\tau_\alpha$, with $G_0 = 8.5$ Pa, vs $\dot{\gamma}$ (dashed line: $\bar{\sigma} \propto \dot{\gamma}^{0.2}$) compared with the macroscopic flow curve $\sigma(\dot{\gamma}_a)$ measured in cone-plate geometry (●). Full line: fit to the Herschel-Bulkley model $\sigma = 1.36\ \text{Pa} + A\dot{\gamma}_a^{0.56}$.

local and global rheology. But this cannot explain the rather larger deviations in Fig. 5. Possibly, the relation $\bar{\sigma} = G_0\tau_\alpha\dot{\gamma}$ is an oversimplification [37] and instead we may need to invoke analogies with "force chain" dominated systems to make progress. Indeed, our *global* shear profile $\dot{\gamma}(z)$, which exhibits a smooth rather than a steplike decay of $\dot{\gamma}(z)$ to zero (data not shown), has similarities with velocity profiles in granular matter [38].

Concluding, we have studied the three-dimensional particle dynamics in a HS colloidal glass under steady shear by fast confocal microscopy. Shear occurs in "fluidized" bands where colloids show nearly isotropic "cage breaking" and exponential relaxation, in contrast to the stretched-exponential dynamics in dense colloidal fluids. The relaxation rate scales as a power of the *local* shear rate: $\tau_\alpha^{-1} \propto \dot{\gamma}^{0.8}$. The "naïve" microscopic flow curve deduced from this result differs from the global, Herschel-Bulkley, rheology. These and other recent results [39] show the potential of fast 3D imaging to address fundamental questions in nonequilibrium physics.

We thank M. E. Cates, M. Fuchs, L. Isa, A. Morozov, P. N. Pusey, K. S. Schweizer, and F. Varnik for discussions, M. Jenkins for providing his coordinate refinement routine, and EPSRC No. GR/S10377 and No. EP/D067650 (U.K.) and NSF No. DMR-0603055 (U.S.) for funding.

[1] M. D. Ediger *et al.*, J. Phys. Chem. **100**, 13 200 (1996).
[2] M. Heggen *et al.*, J. Appl. Phys. **97**, 033506 (2005); H. Kato *et al.*, Appl. Phys. Lett. **73**, 3665 (1998).
[3] R. G. Larson, *The Structure and Rheology of Complex Fluids* (Oxford University Press, New York, 1999).
[4] P. Sollich *et al.*, Phys. Rev. Lett. **78**, 2020 (1997).
[5] L. Berthier, J. Phys. Condens. Matter **15**, S933 (2003).
[6] M. Fuchs and M. E. Cates, Phys. Rev. Lett. **89**, 248304 (2002); Faraday Discuss. **123**, 267 (2003).
[7] M. L. Falk and J. S. Langer, Phys. Rev. E **57**, 7192 (1998).
[8] R. Yamamoto and A. Onuki, Phys. Rev. E **58**, 3515 (1998); Phys. Rev. Lett. **81**, 4915 (1998).
[9] L. Berthier and J. L. Barrat, J. Chem. Phys. **116**, 6228 (2002).
[10] K. Miyazaki *et al.*, Phys. Rev. E **70**, 011501 (2004).
[11] G. Petekidis *et al.*, Phys. Rev. E **66**, 051402 (2002).
[12] P. Hebraud *et al.*, Phys. Rev. Lett. **78**, 4657 (1997).
[13] J. Lauridsen *et al.*, Phys. Rev. Lett. **93**, 018303 (2004); P. Varadan and M. J. Solomon, J. Rheol. **47**, 943 (2003); D. Derks *et al.*, J. Phys. Condens. Matter **16**, S3917 (2004); I. Cohen *et al.*, Phys. Rev. Lett. **93**, 046001 (2004).
[14] D. Bonn *et al.*, Phys. Rev. Lett. **89**, 015701 (2002).
[15] P. Coussot *et al.*, Phys. Rev. Lett. **88**, 218301 (2002); L. Becu *et al.*, Phys. Rev. Lett. **96**, 138302 (2006).
[16] F. Varnik *et al.*, Phys. Rev. Lett. **90**, 095702 (2003).
[17] Deduced from slow quiescent crystallization kinetics.
[18] A. Yethiraj and A. van Blaaderen, Nature (London) **421**, 513 (2003).
[19] $\sqrt{\langle dy^2\rangle}_{\phi_g} \simeq 0.13a$; for pure HSs [20] $\sqrt{\langle dy^2\rangle}_{\phi_g} \simeq 0.18a$.
[20] W. van Megen *et al.*, Phys. Rev. E **58**, 6073 (1998).
[21] J. C. Crocker and D. G. Grier, J. Colloid Interface Sci. **179**, 298 (1996); M. Jenkins (private communication). At our frame rate, shear distortions in the x, z plane are negligible for $\dot{\gamma} \lesssim 0.05\ \text{s}^{-1}$.
[22] L. Isa *et al.*, J. Phys.: Conf. Ser. **40**, 124 (2006).
[23] P. R. ten Wolde *et al.*, J. Chem. Phys. **104**, 9932 (1996); we find $\langle N_x\rangle \sim 2.5$ crystalline bonds per colloid, and only small crystalline clusters of colloids with $N_x \geq 8$.
[24] B. J. Ackerson and P. N. Pusey, Phys. Rev. Lett. **61**, 1033 (1988); M. D. Haw *et al.*, Phys. Rev. E **57**, 6859 (1998).
[25] E. R. Weeks *et al.*, Science **287**, 627 (2000); W. K. Kegel and A. van Blaaderen, Science **287**, 290 (2000).
[26] R. E. Courtland and E. R. Weeks, J. Phys. Condens. Matter **15**, S359 (2003).
[27] Remarkably, Fig. 3(a) includes two points at lower ϕ, $\phi[10^3\dot{\gamma} = 0.47\,\text{s}^{-1}] \simeq 0.61$ and $\phi[10^3\dot{\gamma} = 1.48\,\text{s}^{-1}] \simeq 0.60$.
[28] H. Horner, Z. Phys. B **100**, 243 (1996).
[29] V. Kobelev and K. S. Schweizer, Phys. Rev. E **71**, 021401 (2005); data replotted from their Figs. 9 and 13.
[30] Taking $\tau_{\alpha,j}$ ($j = x, z$) from $F_s(Q_m \parallel j, t = \tau_{\alpha,j}) = 1/e$.
[31] D. R. Foss and J. F. Brady, J. Fluid Mech. **401**, 243 (1999).
[32] X. Qiu *et al.*, Phys. Rev. Lett. **61**, 2554 (1988).
[33] V. Breedveld *et al.*, J. Chem. Phys. **116**, 10529 (2002).
[34] F. Varnik and O. Henrich, Phys. Rev. B **73**, 174209 (2006).
[35] G. Petekidis *et al.*, J. Phys. Condens. Matter **16**, S3955 (2004).
[36] Thus the correspondence between our *bulk* rheology and the predictions in [4,6] for *uniform* shear is puzzling.
[37] An explanation of the difference between $\sigma(\dot{\gamma}_a)$ and $\bar{\sigma} = G_0\tau_\alpha\dot{\gamma}$ in terms of $G_0 = G_0[\phi(\dot{\gamma})]$ along with $\phi > \phi_0$ (the average volume fraction) in the sheared region faces the difficulty that in the jammed regions we would have $\phi < \phi_0$. Further, shear-induced size segregation is unlikely due to the small measured values of shear-induced migration.
[38] W. Losert *et al.*, Phys. Rev. Lett. **85**, 1428 (2000); E. Aharonov and D. Sparks, Phys. Rev. E **65**, 051302 (2002).
[39] L. Isa *et al.*, Phys. Rev. Lett. **98**, 198305 (2007); I. Cohen *et al.*, Phys. Rev. Lett. **97**, 215502 (2006).